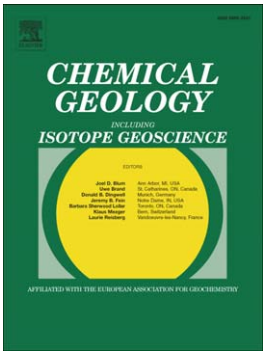

Arsenic-bearing phases in South Andean volcanic ashes: Implications for As mobility in aquatic environments

G. Bia, L. Borgnino, D. Gaiero, M.G. García

PII: S0009-2541(14)00446-X
DOI: doi: 10.1016/j.chemgeo.2014.10.007
Reference: CHEMGE 17371

To appear in: *Chemical Geology*

Received date: 3 July 2014
Revised date: 6 October 2014
Accepted date: 7 October 2014

Please cite this article as: Bia, G., Borgnino, L., Gaiero, D., García, M.G., Arsenic-bearing phases in South Andean volcanic ashes: Implications for As mobility in aquatic environments, *Chemical Geology* (2014), doi: 10.1016/j.chemgeo.2014.10.007

Arsenic-bearing phases in South Andean volcanic ashes: implications for As mobility in aquatic environments

G. Bia, L. Borgnino, D. Gaiero, M. G. García*

Centro de Investigaciones en Ciencias de la Tierra (CICTERRA), CONICET and Universidad Nacional de Córdoba, Argentina.

*Corresponding author. Present address: Av. Vélez Sarsfield 1611 - X5016GCA - Córdoba – Argentina. Tel.: +54 351 5353800.

E-mail address: ggarcía@efn.uncor.edu (M. G. García)

Abstract

Three samples of volcanic ashes collected after eruptions of the volcanos Hudson in 1991, Chaitén in 2008 and Puyehue in 2011 were analyzed in order to define the solid speciation of arsenic and the dynamics of its release to the aqueous phase. The bulk chemical and mineralogical characterization of the samples was performed by ICP/OES, DRX, and SEM/EDS analysis. The chemical composition of the near surface region (first 2-10 nm), along with the As and Fe solid speciation was performed by XPS. Batch experiments were conducted to evaluate the kinetics of the arsenic release under variable pH conditions. The integrated analysis of these data indicate that arsenic compounds are concentrated onto the ash surface in the form of As(III)-S and As(V)-O species. The As(III) species have been assigned to arsenian pyrite, while As(V)-O compounds have been assigned to adsorbed arsenate ions or Fe arsenate salts precipitated as thin coatings.

Although the main As carrier in the studied volcanic ashes is Al-silicate glass, this phase is stable at the neutral pH that dominates the aqueous reservoirs of the area

affected by ashfall. Thus, its contribution to the pool of dissolved arsenic is minor. Higher contributions are clearly associated with the more mobile As species that concentrate onto the surface of Al-silicate glass. This more available arsenic represents less than 6% of the total measured arsenic.

Key Words: XPS, As Solid speciation, Al-silicate glass, South America

1. INTRODUCTION

South America is home to the longest continental volcanic region in the world. Since the Late Triassic, magmatism and volcanism have centered on the Andean region. The first documentation of volcanoes in the region was recorded by the voyages of Columbus and Pizarro in the 16th century. Since then, a large number of volcanoes in the Andes volcanic arc have erupted one or more times (Global Volcanism Program, Smithsonian Institution). In this region, Chile is the country with the largest number of historically active volcanoes. The environmental consequences, however, are mostly observed in neighboring Argentina which is located downwind, and generally receives most of the ashfall. The elevated concentrations of As that are measured in the groundwater of the Chaco-Pampean region (Central and Northern Argentina), have traditionally been assigned to the alteration of volcanic glass spread in the loessic sediments that blanket the entire region (i.e., Nicolli et al. 2012). While most of these conclusions were generated on the basis of water geochemistry analysis, little is known about the As- bearing phases associated with these materials.

Volcanic ash is generally produced by the expansion of magmatic gases. When magma ascends to the Earth's surface and pressure decreases, gases become supersaturated; bubbles nucleate and grow within the magma. The magmatic volatiles

are scavenged by ash particles during their transport in the volcanic plume by gas-particle and liquid-particle interactions (Taylor and Stoiber, 1973; Oskarsson, 1980; Delmelle et al., 2007; Martin et al., 2012). As the erupted plume cools, the volatiles condense onto the ash particle surfaces (Rose, 1977; Rose et al., 1980). Pokrovski et al. (2002) studied the speciation of arsenic in eruptive gases and found that arsenic is predominantly in the form of $As(OH)_3$. Similar to other volatile compounds, $As(OH)_3$ can be adsorbed onto ash surfaces (Allard et al, 2000; Witham et al, 2005) and transported in this form along with the solid. A part of the magmatic arsenic could also be incorporated into the glass structure (i.e., Borisova et al., 2010).. The partial remobilization of structural As can occur by the dissolution of aluminosilicate glass, which is produced under the extreme acid conditions that predominate within the volcanic plume due to the presence of volatile acids (i.e., HCl, H_2S, HF). Along with As, other elements, including Ca, Mg, Na and K, are also released and then precipitated, forming thin coatings onto the glass surfaces (i.e., Rose, 1977; Oskarsson, 1980; Africano and Bernard, 2000; Delmelle et al, 2007; Gislason et al, 2011b).

A number of studies have already documented the relevance of compounds that are formed in the near-surface region of volcanic glasses in the rapid release of hazardous elements and nutrients to aquatic environments (i.e., Witham et al., 2005; Jones and Gíslason, 2008; Ruggeri et al., 2010). The study of the chemical composition of this near-surface region (first 2-10 nanometers) thus becomes key to understanding the mobility of natural contaminants in regions affected by ashfall. X-ray photoelectron spectroscopy (XPS) is a powerful tool used to determine the chemical composition of the top nanometers of solids and to discriminate between the electronic states of the elements. This technique has previously been applied in samples of volcanic ash collected after the eruptions of Eyjafjallajökull (2010), Grímsvötn (2011) and Chaitén

(2008) volcanoes. None of these works reported concentrations of As or its electronic state.

In this study, we report XPS data coupled with a complete chemical and mineralogical characterization of three Andean ashes emitted during recent eruptions. Our aim is to identify the As-bearing phases present in the near-surface region of the glass grains. Kinetics experiments performed under different pH conditions further help us to understand the impact of As release in aqueous reservoirs affected by ash deposition studied here. To the best of our knowledge, this is the first time that surface As-bearing components in Andean volcanic ashes have been identified through the interpretation of XPS spectra.

2. MATERIALS AND METHODS

2.1. Sampling

Three volcanic ash samples were collected a few hours after eruptions of the Chilean volcanos Hudson (1991, 45°S 72°W), Chaitén (2008, 42°S 72°W) and Puyehue (2011, 40°S 72°W). The Hudson ash sample was collected at San Julian, a costal locality 550 km SE of the volcano. The Chaitén sample was collected at the village of Esquel, located at the eastern foot of the Andes about 110 km E of the volcano. Finally, the sample from the Puyehue eruption was collected from the roof of a house in the city of Bariloche 110 km E of the volcano.

After collection, samples were air-dried and sieved through <63 μm mesh in order to separate the silty-clayed fraction. All the results presented here refer to this fraction.

2.2 Chemical and surface characterization

Bulk chemical analysis was carried out on the ground <63 μm fraction by inductively coupled plasma optical emission spectrometry (ICP/OES) after lithium metaborate/tetraborate fusion. The validity of the results for major, minor, and trace elements was checked against measurement of NCS DC70014 standards, which were carried out along with sample analysis.

Grain-size of the volcanic ashes was measured by laser diffraction using a Horiba LA 950 particle size analyzer. Samples were minimally dispersed to prevent the breaking up of aggregates. The precision (reproducibility) of the laser diffraction particle sizer was tested by using mixtures of glass beads (NIST Traceable polydisperse particle standard PS202/3-30 μm and PS215/10-100 μm, Whitehouse ScientificW). For both runs (PS202, n = 6 and PS215, n = 5) the median (D50) was certified to be within 3% of nominal value, and the percentiles D10 and D90 were within 5% of nominal values for the standards.

The specific surface area (SSA) was measured by N_2 adsorption using a computer-controlled STROHLEIN area meter II instrument.

The chemical composition of the near-surface region (2-10 nm) was determined by X-ray photoelectron spectroscopy (XPS) using a XR50, Specs GmbH operated in a hemispherical electron energy analyzer PHOIBOS 100 MCD Specs, with a pass energy of 40 eV and non-monochromatic Mg Kα source (hν = 1253.6 eV; work voltage 13 kV and power 300 W). Air dried samples were analyzed in an ultra-high vacuum (UHV). A two-point calibration of the energy scale was performed using sputtered cleaned gold (Au $4f_{7/2}$, binding energy (BE) = 84.00 eV) and copper (Cu $2p_{3/2}$, BE = 932.67 eV) samples. Broad scans were collected over a 1100-eV range and high resolution spectra were obtained for Al, Si, C, O, Na, Ca, Fe, Cl, P, F, As, S, Mg and K at a resolution of

0.14 eV per step, 200 ms per step and a pass energy of 20 eV. For energy calibration purposes, in order to correct charging effects, all photoelectron peaks (Al 2p, Si 2p, O 1s, Na 1s, Ca 2p, Fe $2p_{3/2}$, Cl 2p, P 2p, F 1s, As 3d, S 2p, Mg 2p and K 2p) were referenced against the C 1s binding energy from the aliphatic contaminants (originating from the hydrocarbon contamination of the surfaces) at 284.8 eV. In order to ensure comparability, the scan procedure was identical for all samples; no evidence of beam damage was found. For chemical composition, data were treated with commercial software, CasaXPS, using Shirley background correction. As and Fe spectra were fitted using the software of XPSpeak 4.1 with peaks of Gaussian-Lorentzian mixed function after subtraction of a Shirley baseline. The full width at half maximum (FWHM) was fixed during the fitting. The FWHMs were 2.0, 2.1 and 2.3 eV for As $3d_{5/2}$, ferrous and ferric species, respectively. In order to provide a reasonable agreement with the measured spectrum, all spectra were fitted with the least number of components possible. Finally, the peaks corresponding to the binding energies (BE) of As and Fe species were identified by comparing them to the reported values.

2.3. Minerological analysis

Minerals present in the <63 μm size-fraction of the samples were identified by X-ray diffraction (XRD) and scanning electron microscopy/energy-dispersive X-ray spectroscopy (SEM/EDS) measures. XRD analysis was performed with a Philips X´Pert PRO X-ray diffractometer operating at 40 kV and 40 mA using Cu-Kα radiation. XRD data were obtained for random samples in the 2θ range from 5 to 70º (step size: 0.02; 13 s/step). The mineralogical interpretation was done using the software X´Pert HighScore, installed on the X-ray diffractometer.

SEM/EDS studies were performed with a JEOL 35 JXA-8230 electron probe microanalyzer coupled with an energy-dispersive X-ray (EDS) analyzer. The samples were prepared in graphite stubs and coated with carbon. In addition, SEM was coupled with focused energy dispersive X-Ray analysis (EDAX DX4), in order to perform the elemental semi-quantification. The detection limit of EDS analysis was about 0.5 % for arsenic; the spatial resolution was about 1 μm.

2.4. Kinetics experiments

Batch experiments were performed in order to evaluate the release of As throughout time under varying pH conditions. The experiments we carried out by suspending ~1.0000 g of dry ash in three solutions consisting of 20 mL of milliQ water in which the pH was initially set at 6.5, 3.0 and 10.0. The pH value of the suspensions was kept constant during the experiments by adding drops of either 0.1 M HNO_3 or NaOH solutions. Aliquots of the suspension were withdrawn after 1.5, 24, 72, 168, 240 and 336 hours from the start of the experiments, centrifuged at 5000 rpm for 15 min and then filtered through a 0.45 μm cellulose membrane filter. Total As and Al contents were analyzed in acidified (1 % HNO_3) dilutions by ICP-MS. Detection limits were 0.22 μg L^{-1} and 2.5 μg L^{-1} for As and Al respectively.

3. RESULTS

3.1. Chemical and mineralogical characteristics of volcanic ashes

Table 1 shows the bulk chemical composition of the three analyzed samples. According to the TAS classification (Le Maitre, 1984), Hudson ashes are trachyandesite in type, while Puyehue show a trachydacitic composition and Chaitén ashes are mainly dacitic. Similar to bulk chemical composition, trace element contents also indicate

compositional differences among the magmatic sources. The content of arsenic is remarkably higher in the Chaitén ashes than those measured in Puyehue and Hudson samples (Table 1). Surface areas for all three samples were lower than 3.5 $m^2 g^{-1}$.

TABLE 1

Observations using SEM/EDS showed that samples mostly consist of abundant shards of glass and small grains of crystalline minerals. Although X-ray diffractograms of the three studied ashes were typical of poorly crystalline materials (Figure 1), minerals such as quartz, plagioclase and cristobalite were identified in the Chaitén and Puyehue samples (Figure 1).

Grain-size distribution in the Hudson ash sample is unimodal, with a peak at ~48 μm diameter. The chemical characterization of single grain minerals allowed for the identification of Ti and Fe (hydr)oxide coatings associated with pyroxene and plagioclase, as well as frequent grains of ilmenite and subhedral to anhedral crystals of pyrite. Occasional halite, gypsum, illite and chromite were also identified. Glass shards show sharp borders and smooth surfaces; their composition is characterized by the dominance of Al, Fe, Ti, Mg, Ca and silica. Very fine particles appear adhered to the glass surface or filling vesicles (Figure 1).

The grain-size distribution in the Chaitén ash is bimodal. The coarsest peak corresponds to ~46 μm diameter while the finest mode corresponds to ~14 μm diameter and is the predominant grain size in the sample. SEM/EDS analysis reveals the presence of Fe and Mn oxides, ilmenite, olivine, and euhedral pyrite. Like Hudson, the ash surface shows abundant vesicles filled with fine particles. Acicular crystals of cristobalite are frequently observed in this sample. The chemical composition of glass is dominated by Al, Na, K and silica, with subordinate amounts of Fe, Mg and Ca (Figure 1).

The most frequent grain-size in the Puyehue ashes was 14 μm. Primary minerals such as andesine, quartz, and cristobalite were recognized by X-ray diffractometry, while minor minerals such as gypsum, Fe (hydr)oxides and cristobalite were identified by EDS mapping. The glass showed a composition dominated by Ca, Na and silica (Figure 1).

No arsenic was detected by EDS analysis, probably because the detection of low levels of this element is not adequate when Mg-bearing minerals are also present, due to the overlap of peaks.

FIGURE 1

3.2. Kinetics experiments

Figure 2 illustrates the results obtained from the kinetics experiments performed on the suspensions of the three ashes in solutions at pH 3.0, 6.5 and 10.0. As observed, the release involves two stages: a first rapid step, which occurs during the first 90 minutes, followed by a second, much slower step that involves a gradual release of As after 300 h, when pseudo-equilibrium conditions are reached. In the first hour of reaction, up to 0.6 % of the bulk As was released into the solution at pH 3.0 and up to 1.1% at pH 10.0. Interestingly, similar amounts of As were released in the first hour of reaction in acidic and basic suspensions, while at pH 6.5 the amount of As released was lower in the three cases. This first step may represent the rapid release of arsenic by desorption and/or dissolution of more soluble As-bearing phases deposited in the uppermost region of the glass grains.

The final concentration of As measured in the leachates at pseudo-equilibrium (after 336 h) showed that As is preferentially released under extreme pH conditions, while at neutral pH, the release is minimized (insets in Figure 2). The final concentration of As in the leachates also seems to be conditioned by the content of total

arsenic in the bulk samples. The Chaitén sample leachates exhibited the highest release, probably because it has been formed from a magmatic source richer in arsenic. The amount of As released at the end of the experiments at pH 3.0, represented 1.7, 11.1 and 1.5 % of the bulk As concentrations determined in the Hudson, Chaitén and Puyehue ashes respectively, while at pH 10.0 the corresponding percentages were 1.9, 9.8 and 3.7%.

FIGURE 2

3.3. Surface composition

The relative element mass concentrations in the fresh surfaces are shown in Table 2 along with the composition of the bulk samples expressed in weight %. Most elements are depleted in the near-surface region, while As and some other elements such as F, Mg and Ca show noticeable enrichments.

TABLE 2

Fig. 3 shows the XPS spectra obtained for As3d bands. Although the signals are relatively weak and noisy, two peaks could be fitted, at ~43.4 eV and ~45.0 eV (Figure 3, Table 3) using a peak separation constrained at 2 eV. Reference values used for peak identification are listed in Table 4. According to these values, peaks at ~43.4 eV identified in Puyehue and Chaitén samples correspond to As(III)-S compounds. The peak at 43.7 eV observed in the Hudson sample was also attributed to As(III) species by comparison with reference BE values reported by Costa et al. (2002). A similar interpretation was applied by Schaufuss et al (2000) to signals observed in XPS spectra of arsenopyrite oxidized surface samples. Peaks fitted at ~45.0 eV correspond to As(V)-O compounds.

FIGURE 3

TABLE 3

TABLE 4

Because the most common phases containing As-S bondings are Fe sulphides, we have also analyzed the XPS spectra corresponding to the $Fe2p_{3/2}$ band (Figure 4). The obtained peaks (Table 3) coincide with the BE of the following chemical bondings: Fe(II)-AsS, Fe(II)-O, and Fe(III)-O. In accordance with values reported in the literature (Table 4), the peaks found in the range between 706 and 708 eV are typical of Fe-S bondings, which are usually assigned to pyrite (i.e., Nesbitt et al., 1995; Costa et al., 2002). However, Nesbitt et al (1995) demonstrated that Fe-As-S and Fe-S-S bondings have the same BE in XPS spectra obtained from loellingite ($FeAs_2$) and pyrite crystals. Binding energies for Fe(II)-O are near 709 eV (Costa et al., 2002) while for Fe(III)-O are in the range of 711-712 eV (Eggleston et al. 1996), which is suggestive of the presence of Fe (hydr)oxides.

FIGURE 4

4. IDENTIFICATION OF AS-BEARING PHASES

In this section we analyze the possible As-bearing phases in detail.

4.1. Structural As in the Al-silicate glass

Recent studies have investigated the speciation and structure of arsenic in natural melts and glasses. They found that oxy-hydroxide complexes such as $AsO(OH)_2^-$ and/or $As(OH)_3$ are the primary As species in these systems (e.g., Pokrovski et al., 2002; Testemale et al., 2004; Borisova et al., 2010; James-Smith et al., 2010). These findings indicate that this element may form strong bonds within the glass structure and thus, extreme chemical conditions (i.e.: strongly acidic or alkaline media) are necessary to release these atoms to the water.

The results obtained from kinetics experiments reveal that As is preferentially released under extreme pH conditions which suggests, on the basis of previous works, that the dissolution of glass is taking place. Declercq et al. (2013) summarized the dissolution of natural Al-silicate glasses as a series of steps that begins by the rapid exchange of protons for alkali and alkaline-earth metals near the glass surface leading to the formation of an Al and Si-rich surface layer (Thomassin and Touray, 1979; Berger et al., 1987; Guy and Schott, 1989; Gout et al., 1997; Crovisier et al., 2003; Oelkers et al., 2009). The final, rate-limiting step of natural Al-silicate glass dissolution is the destruction of this Si- and Al-rich surface layer (Daux et al., 1997; Oelkers and Gislason, 2001; Gislason and Oelkers, 2003; Wolff-Boenisch et al., 2004a,b). On the basis of kinetics experiments and numerical modeling, Gıslason and Oelkers (2003) predicted the dissolution rates of basaltic glass across the entire range of pH. According to their calculations, at 25ºC minimum rates of dissolution were determined at pH ~6. At lower pH values, rates steeply increase (about 4 orders of magnitude higher at pH 2) while under more alkaline conditions, the increase is more moderate (about 2 orders of magnitude higher at pH 10.0). Equations 1 and 2 represent the dissolution of the Al-silicate glass occurring under acidic and alkaline condition respectively, as indicated by Oelkers and Gíslason (2001).

$$SiAl_{0.36}O_2(OH)_{1.08} + 1.08H^+ \leftrightarrow SiO_{2(}aq) + 0.36Al^{3+} + 1.08\ H_2O \quad (1)$$

$$2.77\ SiAl_{0.36}O_2(OH)_{1.08} + 0.33OH^- + 3H_2O = Al(OH)_4^- + 2.77\ SiO_{2(}aq) \quad (2)$$

The solid curve shown in Figure 5 represents the concentration of Al released after the dissolution of basaltic glasses at 25ºC as predicted by the rate law of Gíslason and Oelkers (2003). Our experimental data were also plotted; as seen in the figure, the experimental trends closely resemble the theoretical curve, which suggests that dissolution of the Al-silicate glass is actually taking place in our systems, especially

after the first 90 min, when the kinetics of the As release began to slow. This trend thus reinforces the hypothesis that when extreme pH conditions predominate, As is released from sites within the glass structure.

FIGURE 5

4.2. Surface As speciation in the Al-silicate glass

The first rapid release of As determined in the kinetic experiments likely corresponds to soluble As-bearing phases concentrated at the near surface region of the studied glasses. These phases are As(III)-S and As(V)-O compounds, as it was determined from the deconvolution of XPS spectra for the As 3d band (Figure 3).

Since no single phases containing detectable concentrations of As and S were found through SEM/EDS analysis, As(III)-S species could be assigned to arsenic occurring as a trace impurity in sulphide minerals, particularly pyrite. Abraitis et al. (2004) reported that pyrite may incorporate up to ca. 10.0 wt% of arsenic within its structure. The arsenic-bearing pyrite is known as arsenian pyrite; it is found in low-temperature hydrothermal environments, especially sedimentary basins and mineral deposits (Wells and Mullens, 1973; Savage et al., 2000; Kolker et al., 2003). Previous studies of arsenian pyrite have shown that As substitutes as As^{1-} for S in the S_2^{2-} unit to form $Fe(As^{1-},S)_2$ (e.g., Fleet et al., 1989; Fleet and Mumin, 1997; Simon et al., 1999; Pals et al., 2003; Zachariáš et al., 2004; Reich et al., 2005). In a more recent study, Chouinard et al., (2005) suggested that As^{3+} may substitute for Fe^{2+} in arsenian pyrite from the Pascua Lama deposit (Chile). This substitution was also determined by Deditius et al (2008) by using XPS, HRTEM, and EMPA analyses in microcrystals of arsenian pyrite collected from hydrothermal deposits in Perú.. We have not observed the peak of As^{1-} in the As3d XPS spectra. Therefore, we consider that the As(III)-S bonding

may correspond to the presence of microcrystals of As(III)-pyrite. This statement is further supported by the identification of Fe-As-S species in the Fe2p XPS spectra recorded for our samples (Figure 4). In fact, single crystals of cubic pyrite were observed in Hudson ashes, while in Chaitén, amorphous Fe-S coatings have been determined by ESD mapping (Figure 6).

FIGURE 6

Finally, peaks found in the region near 45.0 eV correspond to As(V)-O bondings (i.e., Nesbitt et al., 1995; Nesbitt and Muir., 1998; Fullston et al., 1999; Schaufuss et al., 2000; Costa et al., 2002; Kim et al., 2014). They can be assigned to arsenate present at the glass surface as adsorbed and/or precipitated as poorly crystalline scorodite-like phase formed by oxidative dissolution of As-bearing sulphides (i.e., Asta et al., 2010; Courtin-Nomade et al., 2010).

5. ENVIRONMENTAL IMPLICATIONS FOR AQUATIC SYSTEMS

Volcanic ash is the most widely-distributed product of explosive volcanic eruptions, and ashfall may affect areas hundreds of kilometers away from an erupting volcano (Stewart et al., 2006). South America is particularly affected by this phenomenon, as it spans the greatest length of any continental volcanic region in the world (Global Volcanism Program, Smithsonian Institution). Historical records of volcanic eruptions in the region are only available after ~500 years BP. The largest eruptions recorded during the 20th century took place in Chilean volcanoes (i.e., Quizapu, 1932; Hudson, 1991) and produced heavy ashfall that drifted downwind to the east. Distal ashfall was reported in regions as far as Rio Janeiro, Brazil (Quizapu eruption; González-Ferrán, 1995) and the Malvinas Islands in the South Atlantic Ocean

(Hudson eruption; Tilling, 2009). The 1991 Hudson eruption ejected ~4.3 km^3 of ash (Scasso et al., 1994) and caused heavy ashfall southeast of the volcano.

More recent eruptions registered in the Patagonia region also delivered important volumes of ashfall to nearby regions. The most remarkable include the 2008 eruption of the Chilean volcano Chaitén, which deposited a volume of ~0.15 km^3 of tephra (Watt et al., 2009) over Argentina, and the 2011 eruption of the Puyehue-Cordón Caulle volcanic complex, which ejected ~0.12 km^3 of volcanic material. In May 2008, the Chaitén volcano erupted explosively and produced an ash plume that rose 21 km into the atmosphere (Lara, 2009; Carn et al., 2009). Heavy ashfall from the plumes affected extensive downwind areas of neighboring Argentina (e.g., Folch et al., 2008; Martin et al., 2009; Watt et al., 2009). On June 4th 2011, the Puyehue volcano began an eruptive process, generating a column made of gases and volcanic ash 11-13 km high and 5 km wide. The eruption dispersed volcanic products to the SE of the volcano, reaching the Atlantic Ocean coast in just one day. In the following days, the dispersion of the volcanic plume had varied in direction, but predominantly moved to the east side of the Andean mountains based on the dominant west-east wind currents at this latitude (Daga et al., 2014).

These recent eruptions are only a brief sample of the more important eruptions in southern Patagonia, which reveal the magnitude of ashfall that has affected large regions in the southern portion of South America, delivering hazardous elements and compounds of magmatic origin. At the place of deposition, a rapid dissolution of the more soluble phases is most likely to occur. In contrast, the dissolution of the glassy fraction is expected to be slower, as the dissolution of silicate glass is produced at low rates for the pH conditions that dominate most aquatic reservoirs in the affected areas. Initial chemical fluxes into these aquatic environments will thus be derived from the

rapid dissolution/detachment of the more mobile phases (As(III) and As (V) surface species) present on the glass surfaces. In a following stage, the fluxes of As will be dominated by the release of the structural As. These conclusions are mostly derived from the leaching experiments carried out with suspensions of the volcanic ashes in milliQ water, which may better represent the environmental conditions dominating the affected areas.

A hypothetical calculation of the maximun amount of As delivered towards surrounding regions after the analyzed eruptions was performed by using the experimental results in conjunction with data reported in the literature. Table 5 shows the mass of volcanic material emitted by the Hudson, Chaitén and Puyehue volcanoes in the events of 1991, 2008 and 2011 respectively, along with the mass of total As delivered in each eruptive event, estimated from the concentration of bulk As in the studied ashes. The table also includes the estimations of the amount of As potentially released from the deposited ashes after 90 minutes and 14 days of exposure to water (considering that the entirety of the ash would be submerged/exposed to water). All these amounts represent less than ~6% of the bulk As measured in the ash samples (Table 4).

TABLE 5

In the vast Chacopampean plain, groundwater resources exhibit concentrations of arsenic that largely exceed national and international guidelines for drinking water (from 470 to 770 μg/L, Nicolli et al., 2012). There is a wide agreement that these elevated concentrations of As, along with other trace elements such as F, Mo, V and U, are derived from the alteration of volcanic glass spread in the loessic sediments that blanket the entire region (i.e. Nicolli et al., 2012). However, the identification of the surface speciation of As in these materials has not yet been performed. Although the

ashes studied here are not those incorporated into the loessic matrix, we may infer that the identified As-bearing phases were also present in ashes that had been emitted by past eruptions and then deposited into the Chacopampean Plain. If this is true, the old volcanic ashes would have rapidly released the As associated with As(V)-O and probably As(III)-S compounds during their first exposure to water, while the As included within the glass structure remained almost immobile. Because pH conditions in the aquifers are dominantly neutral to alkaline, the rate of dissolution of silicate glass is low, and thus only a minor proportion of the structural As is released to groundwater. Once in solution, the aqueous species of As interacted with the reactive phases present in the sediments, either adsorbing onto Fe (hydr)oxide coatings or co-precipitating with carbonates, as has been suggested in a previous work (Garcia et al., 2014). From that moment on, the interaction of soluble As with solid particles remained controlled by the geochemical conditions that dominate the aquifer.

6. CONCLUSIONS

Volcanic ashes have been traditionally considered important carriers of arsenic to aquatic environments affected by volcanic ashfall. The identification of the As species associated with this material is thus essential to understanding the dynamics of this pollutant.

The arsenic-bearing phases defined in this work are closely linked with the release of this element to the aqueous media. The most available species are those concentrated onto the grain surface, consisting of thin coatings of As(III)-S compounds, probably arsenian pyrite, and As(V)-O compounds, present as adsorbed/precipitated arsenate species. The most stable As-bearing phase is the Al-silicate glass, where As is included within the structure. The release from this phase at the pH conditions

dominating the aqueous reservoirs represents less than 1% of the total arsenic measured in the bulk samples, while more mobile surficial phases may release up to 6%.

ACKNOWLEDGEMENTS

Authors wish to acknowledge the assistance of CONICET and UNC whose support facilities and funds were used in this investigation. G. Bia acknowledges a doctoral fellowship from CONICET. L. Borgnino, D. Gaiero, and M.G. Garcia are members of CICyT in CONICET, the National Science Foundation of Argentina. We thank Dr. G. Benitez (INIFTA-CONICET) for his assistance in the interpretation of the XPS spectra. Language assistance by native English speaker Wendy Walker is gratefully acknowledged. We are especially grateful to two anonymous reviewers for suggesting significant improvements to this manuscript.

REFERENCES

Abraitis P.K., Pattrick R.A.D., Vaughan D.J. (2004) Variations in the compositional, textural and electrical properties of natural pyrite: a review. *International Journal of Mineral Processing* **74**, 41-59.

Africano F. and Bernard A. (2000) Acid alteration in the fumarolic environment of Usu volcano, Hokkaido, Japan. *J. Volcanol. Geotherm. Res.* **97**, 475–495.

Allard P., Aiuppa A., Loyer H., Carrot F., Gaudry A., Pinte G., Michel A. and Dongarra G. (2000) Acid gas and metal emission rates during long-lived basalt degassing at Stromboli volcano. *Geophys. Res. Lett.* **27**, 1207–1210.

Aradóttir E.S.P., Sigfússon B., Sonnenthal E.L., Björnsson G., Jónsson H. (2013) Dynamics of basaltic glass dissolution – Capturing microscopic effects in continuum scale models. *Geochim. et Cosmochim. Acta*. **121**, 311–327.

Asta M. P., Cama J., Ayora C., Acero P., De Giudici G. (2010) Arsenopyrite dissolution rates in O2-bearing solutions. *Chem. Geol.* **273**, 272–285.

Berger G., Schott J. and Loubet M. (1987) Fundamental processes controlling the 1st stage of alteration of a basalt glass by seawater – an experimental study between 200 and 320 ºC. *Chem. Geol.* **71**, 297–312.

Biesinger M. C., Payne B. P., Grosvenor A. P., Lau L. W.M.,. Gerson A. R, Smart R. St.C. (2011) Resolving surface chemical states in XPS analysis of first row transition metals, oxides and hydroxides: Cr, Mn, Fe, Co and Ni. *Appl. Surface Science.* **257**, 2717–2730.

Borisova A. Y., Pokrovski G.S., Pichavant M., Freydier R., and Candaudap F. (2010) Arsenic enrichment in hydrous peraluminous melts: Insights from femtosecond laser ablation-inductively coupled plasma-quadrupole mass spectrometry, and in situ X-ray absorption fine structure spectroscopy. *American Mineralogist*. **95**, 1095–1104.

Carn S. A., Pallister J. S., Lara L., Ewert J. W., Prata A. J., Thomas R. J., and Villarosa G. (2009) The unexpected awakening of Chaitén Volcano, Chile. *Eos, Transactions American Geophysical Union*. **90**, 205–212.

Chouinard A., Paquette J. and Williams-Jones A. E. (2005) Crystallographic controls on trace-element incorporation in auriferous pyrite from the Pascua epithermal high-sulfidation deposit, Chile–Argentina. *Can. Mineral.* **43**, 951–963.

Corkhill C.L. and Vaughan D.J. (2009) Arsenopyrite oxidation – A review. *Applied Geochemistry*. **24**, 2342–2361.

Costa M.C., Botelho do Rogo A.M., Abrantes L.M. (2002) Characterisation of a natural and an electro-oxidised arsenopyrite: a study on electrochemical and Xray photoelectron spectroscopy. *Int. J. Miner. Process*. **65**, 83–108.

Courtin-Nomade A., Bril H., Bény J., Kunz M., Tamura N. (2010) Sulfide oxidation observed using micro-Raman spectroscopy and micro-X-ray diffraction: The importance of water/rock ratios and pH conditions. *American Mineralogist*. **95**, 582–591.

Crovisier J. L., Honnorez J., Fritz B. and Petit J. C. (1992) Dissolution of subglacial volcanic glasses from Iceland – laboratory study and modeling. *Appl. Geochem.* **7**, 55–81.

Crovisier J. L., Advocat T. and Dussossoy J. L. (2003) Nature and role of natural alteration gels formed on the surface of ancient volcanic glasses (Natural analogues of waste containment glasses). *J. Nucl. Mater*. **321**, 91–109.

Daga R., Ribeiro Guevara S., Poire D.G., and Arribére M., (2014) Characterization of tephras dispersed by the recent eruptions of volcanoes Calbuco (1961), Chaitén (2008) and Cordón Caulle Complex (1960 and 2011), in Northern Patagonia. *Journal of South American Earth Sciences*. **49**, 1-14.

Daux V., Guy C., Advocat T., Crovisier J. L. and Stille P. (1997) Kinetic aspects of basaltic glass dissolution at 90 ºC: role of aqueous silicon and aluminium. *Chem. Geol.* **142**, 109–126.

Declercq J., Diedrich T., Perrot M., Gislason S.R., and Oelkers E. H. (2013) Experimental determination of rhyolitic glass dissolution rates at 40–200º C and 2 < pH < 10.1. *Geochim. Cosmochim. Acta*. **100**, 251–263.

Deditius A. P., Utsunomiya S., Renock D., Ewing R. C., Ramana C. V., Becker U., Kesler S. E. (2008) A proposed new type of arsenian pyrite: Composition, nanostructure and geological significance. *Geochim. et Cosmochim. Acta*. **72**, 2919–2933.

Delmelle P., Lambert M., Dufrene Y., Gerin P., Oskarsson N. (2007) Gas/aerosol–ash interaction in volcanic plumes: new insights from surface analyses of fine ash particles. *Earth and Planet. Sci. Lett*. **259**, 159–170.

Descostes M., Mercier F., Thromat N., Beaucaire C., Gautier-Soyer M. (2000) Use of XPS in the determination of chemical environment and oxidation state of iron and sulfur samples: constitution of a data basis in binding energies for Fe and S reference compounds and applications to the evidence of surface species of an oxidized pyrite in a carbonate medium. *Appl. Surface Science*. **165**, 288–302.

Durant A.J., Villarosa G., Rose W., Delmelle P., Prata A.J., Viramonte J.G. (2012) Longerange volcanic ash transport and fallout during the 2008 eruption of Chaitén volcano, Chile. *Phys. Chem. Earth.* **45-46**, 50-64.

Eggleston C.M., Ehrhardt J.J., Stumm W. (1996) Surface structural controls on pyrite oxidation kinetics: An XPS-UPS, STM, and modeling study. *Am. Mineral.* **81**, 1036–1056.

Folch A., Jorba O., and Viramonte J. (2008) Volcanic ash forecast application to the May 2008 Chaitén eruption. *Nat. Hazards Earth Syst. Sci.* **8**, 927–940.

Fleet M. E., MacLean P. J. and Barbier J. (1989) Oscillatory-zoned As-bearing pyrite from strata-bound and stratiform gold deposits: an indicator of ore fluid evolution. *Econ. Geol. Monogr*. **6**, 356–382.

Fleet M. E. and Mumin A. H. (1997) Gold-bearing arsenian pyrite and marcasite and arsenopyrite from Carlin Trend gold deposits and laboratory synthesis. *Am. Mineral.* **82**, 182–193.

Fullston, D., Fornasiero, D., Ralston, J. (1999) Oxidation of synthetic and natural samples of enargite and tennantite: 2. X-ray photoelectron spectroscopic study. *Langmuir*. **15**, 4530– 4536.

Garcia M.G., Borgnino L., Bia G., Depetris P. J. 2014. Mechanisms of arsenic and fluoride release from Chacopampean sediments (Argentina). *International Journal of Environment and Health*. **7**, 41-57.

Gislason S. R. and Oelkers E. H. (2003) The mechanism, rate and consequence of basaltic glass dissolution: II. An experimental study of the dissolution rates of basalts as a function of pH at temperatures from 6ºC to 150ºC. *Geochim. Cosmochim. Acta*. **67**, 3817–3832.

Gislason S. R., Alfredsson H. A., Eiriksdottir E. S., Hassenkam T. and Stipp S. L. S. (2011a) Volcanic ash from the 2010 Eyjafjallajo¨kull eruption. *Appl. Geochem.* **26**, S188–S190.

Gislason S. R., Hassenkam T., Nedel S., Bovet N., Eiriksdottir E. S., Alfredsson H. A., Hem C. P., Balogh Z. I., Dideriksen K., Oskarsson N., Sigfusson B., Larsen G. and Stipp S. L. S. (2011b) Characterization of Eyjafjallajo¨kull volcanic ash particles and a protocol for rapid risk assessment. *Proc. Natl. Acad. Sci. U.S.A.* **108**, 7307–7312.

González-Ferrán O. (1995) Volcanes de Chile: Instituto Geográfico Militar, Santiago, Chile, 639 pp.

Gout R., Oelkers E. H., Schott J. and Zwick A. (1997) The surface chemistry and structure of acid leached albite: new insights on the dissolution mechanism of the alkali feldspars. *Geochim. Cosmochim. Acta*. **61**, 3013–3018.

Guy C. and Schott J. (1989) Multisite surface reaction versus transport control during the hydrolysis of a complex oxide. *Chem. Geol.* **78**, 181–204.

Hacquard E., Bessiere J., Alnot M., Ehrdhardt J.J. (1999) Surface spectroscopic study of the adsorption of Ni(II) on pyrite and arsenopyrite at pH 10. *Surf. Interface Anal.* **27**, 849–860.

Henderson G.S., Calas G. and Stebbins J.F. (2006) The structure of silicate glasses and melts. *Elements*. **2**, 269-273.

James-smith J., Cauzid J., Testemale D., Liu W., Hazemann J-L., Proux O., Etschmann, B., Philippot P., Banks D., Williams P. and Brugger J. (2010) Arsenic speciation in fluid inclusions using micro-beam X-ray absorption spectroscopy. *American Mineralogist*. **95**, 921–932.

Jones M. T. and Gislason S. R. (2008) Rapid releases of metal salts and nutrients following the deposition of volcanic ash into aqueous environments. *Geochim. Cosmochim. Acta*. **72**, 3661–3680.

Kim E.J., Yoo J.-C., Baek K. (2014) Arsenic speciation and bioaccessibility in arsenic-contaminated soils: Sequential extraction and mineralogical investigation. *Environmental Pollution*. **186**, 29-35.

Kolker A., Haack S. K., Cannon W. F., Westjohn D. B., Kim M. J., Nriagu J. and Woodruff L. G. (2003) Arsenic in southeastern Michigan. In Arsenic in Ground Water (eds. A. H. Welch and K. G. Stollenwerk). *Kluwer Academic Publishers, Boston*, pp. 281–294.

Lara L. E. (2009) The 2008 eruption of Chaiten Volcano, Chile: A preliminary report, *Andean Geology*. **36**, 125–129.

Le Maitre R.W. (1984). A proposal by the IUGS Subcommission on the Systematics of Igneous Rocks for a chemical classification of volcanic rocks based on the total alkali silica (TAS) diagram. *Australian Journal of Earth Sciences.* **31**(2), 243-255.

Martin R. S., Watt S. F. L., Pyle D. M., Mather T. A., and Matthews N. E. (2009) Environmental effects of ashfall in Argentina from the 2008 Chaitén volcanic eruption. *J. Volcanol. Geoth. Res.* **184**, 462–472.

Martin R. S., Wheeler J. C., Ilyinskaya E., Braban C. F. and Oppenheimer C. (2012) The uptake of halogen (HF, HCl, HBr and HI) and nitric (HNO3) acids into acidic sulphate particles in quiescent volcanic plumes. *Chem. Geol.* **296–297**, 19–25.

McIntyre N.S., Zetaruk D.G. (1977) X-ray photoelectron spectroscopic studies of iron oxides. *Anal. Chem.* **49**, 1521–1529.

Mills P. and Sullivan J.L. (1983) A study of the core level electrons in iron and its three oxides by means of x-ray photoelectron spectroscopy. *J. Phys. D: Appl. Phys.* **16**, 723–732.

Nesbitt H.W., Muir I.J. (1998) Oxidation states and speciation of secondary products on pyrite and arsenopyrite reacted with mine waste waters and air. *Mineral. Petrol.* **62**, 123–144.

Nesbitt H.W., Muir I.J., Pratt A.R. (1995) Oxidation of arsenopyrite by air and airsaturated, distilled water and implications for mechanisms of oxidation. *Geochim. Cosmochim. Acta*. **59**, 1773–1786.

Nicolli HB., Bundschuh J., Blanco M. del C., Tujchneider O. C., Panarello H. O., Dapeña C., Rusansky J. E. (2012) Arsenic and associated trace-elements in groundwater from the Chaco-Pampean plain, Argentina: Results from 100 years of research. *Science of The Total Environment*. **429**, 36-56.

Oelkers E. H. and Gislason S. R. (2001) The mechanism, rates, and consequences of basaltic glass dissolution: I. An experimental study of the dissolution rates of basaltic glass as a function of aqueous Al, Si, and oxalic acid concentration at 25ºC and pH = 3 and 11. *Geochim. Cosmochim. Acta*. **65**, 3703–3719.

Oelkers E. H., Golubev S. V., Chairat C., Pokrovsky O. S. and Schott J. (2009) The surface chemistry of multi-oxide silicates. *Geochim. Cosmochim. Acta*. **73**, 4617–4634.

Olsson J., Stipp S.L.S., Dalby K.N., Gislason S.R. (2013) Rapid release of metal salts and nutrients from the 2011 Grímsvötn, Iceland volcanic ash. *Geochim. Cosmochim. Acta*. **123**, 134–149.

Oskarsson N. (1980) The interaction between volcanic gases and tephra: fluorine adhering to tephra of the 1970 Hekla eruption. *J. Volcanol. Geotherm. Res.* **8**, 51–266.

Pals D. W., Spry P. G. and Chryssoulis S. (2003) Invisible gold and tellurium in arsenic-rich pyrite from the Emperor gold deposit, Fiji: implications for gold distribution and deposition. *Econ. Geol.* **98**, 479–493.

Pillai Y., Bockris Y. (1985) X-ray photoelectron spectroscopy studies of xanthate adsorption on pyrite mineral surfaces. *J. Colloid Interface Sci.* **103**, 145– 153.

Pokrovski G.S., Zakirov I.V., Roux J., Testemale D., Hazemann JL., Bychkov A.Y., and Golikova G.V. (2002) Experimental study of arsenic speciation in vapor phase to 500 °C: Implications for As transport and fractionation in low-density crustal fluids and volcanic gases. *Geochim. Cosmochim. Acta.* **66**, 3453–3480.

Reich M., Kesler S. E., Utsunomiya S., Palenik C. S., Chryssoulis S. L. and Ewing R. C. (2005) Solubility of gold in arsenian pyrite. *Geochim. Cosmochim. Acta*. **69**, 2781–2796.

Rose WI. (1977) Scavenging of volcanic aerosol by ash: atmospheric and volcanologic implications. *Geology*. **5**, 621–624.

Rose WI., Chuan RL., Cadle RD., Wood DC., (1980) Small particles in volcanic eruption clouds. *Am. J. Sci*. **280**, 671–696.

Ruggieri F., Saavedra J., Fernandez-Turiel J.L., Gimeno D., Garcia-Valles M. Environmental geochemistry of ancient volcanic ashes. *Journal of Hazardous Materials 2010*. **183**, 353–365.

Savage K. S., Tingle T. N., O'Day P. A., Waychunas G. A. and Bird D. K. (2000) Arsenic speciation in pyrite and secondary weathering phases, Mother Lode gold district. Tuolumne County, California. *Appl. Geochem*. **15**, 1219–1244.

Scasso R., Corbella H., Tiberi P. (1994) Sedimentological analysis of the tephra from the 12-15 August 1991 eruption of Hudson volcano. *Bulletin of Volcanology*. **56**, 121-132.

Schaufuss A.G., Nesbitt H.W., Sciani M.J., Hoecsht H., Bancroft M.G., Szargan R. (2000) Reactivity of surface sites on fractured arsenopyrite (FeAsS) toward oxygen. *Am. Mineral.* **85**, 1754–1766.

Simon G., Huang H., Penner-Hahn J. E., Kesler S. E. and Kao L.- S. (1999) Oxidation state of gold and arsenic in gold-bearing arsenian pyrite. *Am. Mineral.* **84**, 1071–1079.

Stewart C., Johnston D.M., Leonard G.S., Horwell C.J., Thordarson T., Cronin S.J. (2006) Contamination of water supplies by volcanic ashfall: a literature review and simple impact modeling. *J. Volcanol. Geoth. Res.* **158**, 296-306.

Taylor P. S. and Stoiber R. E. (1973) Soluble material on ash from active Central American volcanoes. *Geol. Soc. Am. Bull.* **84**, 1031–1041.

Testemale D., Hazemann J.-L., Pokrovski G.S., Joly Y., Roux J., Argoud R., and Geaymond O. (2004) Structural and electronic evolution of the $As(OH)_3$ molecule in high temperature aqueous solutions: An X-ray absorption investigation. *Journal of Chemical Physics.* **121**, 8973–8982.

Tilling R.I. (2009) Volcanism and associated hazards: the Andean perspective. *Advances in Geosciences*. **22**, 125–137.

Thomassin J. H. and Touray J. C. (1979) Early stages of waterbasaltic glass interaction – X-ray photo-electrons spectroscopy (XPS) and scanning electron-microscopy (SEM) investigations. *Bull. Miner*. **102**, 594–599.

Wagner C.D., Riggs W.M., Davis L.E., Moulder J.F., Muilenberg G.E., (1979) Handbook of X-ray Photoelectron Spectroscopy. Perkin–Elmer.

Watt S. F. L., Pyle D. M., Mather T. A., Martin R. S., and Matthews N. E.(2009) Fallout and distribution of volcanic ash over Argentina following the May 2008 explosive eruption of Chaitén, Chile. *J. Geophys. Res*. **114**. B04207, doi:10.1029/2008JB006219.

Wells J. D. and Mullens T. E. (1973) Gold-bearing arsenian pyrite determined by microprobe analysis, Cortez and Carlin gold mines, Nevada. *Econ. Geol*. **68**, 187–201.

Witham C. S., Oppenheimer C. and Horwell C. J. (2005) Volcanic ash-leachates: a review and recommendations for sampling methods. J. Volcanol. *Geotherm. Res*. **141**, 299–326

Wolff-Boenisch D., Gislason S. R., Oelkers E. H. and Putnis C. V. (2004a) The dissolution rates of natural glasses as a function of their composition at pH 4 and 10.6, and temperatures from 25 to 74ºC. *Geochim. Cosmochim. Acta*. **68**, 4843–4858.

Wolff-Boenisch D., Gislason S. R. and Oelkers E. H. (2004b) The effect of fluoride on the dissolution rates of natural glasses at pH 4 and 25ºC. *Geochim. Cosmochim. Acta*. **68**, 4571–4582.

Zachariáš J., Frýda J., Paterová B. and Mihalievič M. (2004) Arsenopyrite and As-bearing pyrite from the Roudny´ deposit, Bohemian Massif. *Mineral. Mag.* **68**, 31–46.

FIGURE CAPTIONS

Figure 1. Electron images, EDS spectra, XRD patterns and grain-size distribution of the studied volcanic ashes. Quartz (Qtz), plagioclase (Pl), cristobalite (Crs), lepidolite (Lpd) and fluorapatite (F-Ap). Scale bars in SEM images correspond to 10 μm in Hudson and Puyehue and to 100 μm in Chaitén samples.

Figure 2. Kinetics curves showing the release of As with time. The insets show the As released after 336 h of reaction as a function of pH. Circles: milliQ water; triangles: pH 3; squares: pH 10.

Figure 3. X-ray photoelectron As 3d spectra obtained for Hudson, Chaitén and Puyehue ashes. The best fit curve is shown by a solid thick line; individual As $3d_{5/2}$ peaks are indicated with dashed lines.

Figure 4. X-ray photoelectron Fe 2p spectra obtained for Hudson, Chaitén and Puyehue ashes. The best fit curve is shown by a solid thick line; individual Fe $2p_{3/2}$ peaks are indicated by dashed lines.

Figure 5. Plot showing the log $Al_{released}$ as a function of pH in leachates obtained after 336 h of suspension. Solid thick line: theoretical dissolution of basaltic glass (Aradottir et al., 2013); dashed lines: experimental results. Squares: Hudson; circles: Chaiten; triangles: Puyehue.

Figure 6. (1) SEM image showing the presence of coatings of Fe-S onto a Al-silicate grains of glass in the Chaitén sample. EDS diagrams show the chemical composition of

two different points in the image. Mappings show the spatial distribution of Si, S and Fe. (2) SEM image and EDS diagram of pyrite found in the Hudson sample.

TABLE CAPTIONS

Table 1. Bulk chemical composition (ICP/OES), specific surface area (BET-N_2) and content of glass determined for the studied samples.

Table 2. Bulk (ICP/OES) and surface (XPS) chemical composition (expressed in weight %) determined for ash samples. Carbon and oxygen contamination, detected on all surfaces, were excluded for a clearer comparison. Enriched elements on particles surface are marked in bold. Conversion of surface concentrations from atoms % in weight % was performed with the online software available from http://www.lasurface.com/xps/convertisseur.php# (Thermofisher Scientific)

Notes to Table 2

S/B, ratio surface/bulk composition. ND, not determined; BDL, below detection limit. F was estimated from the maximum concentration released in the kinetics experiments.

Table 3. As 3d binding energy assignments for the analyzed samples.

Table 4. As $3d_{5/2}$ and Fe $2p_{3/2}$ binding energy values from a compilation of literature sources.

Table 5. Maximum amount of As delivered from the ejected materials during eruptions of Hudson (1991), Chaitén (2008) and Puyehue (2011) volcanoes and amounts of As potentially released after 1.5 h and 14 days of exposure to water.

Figure 1

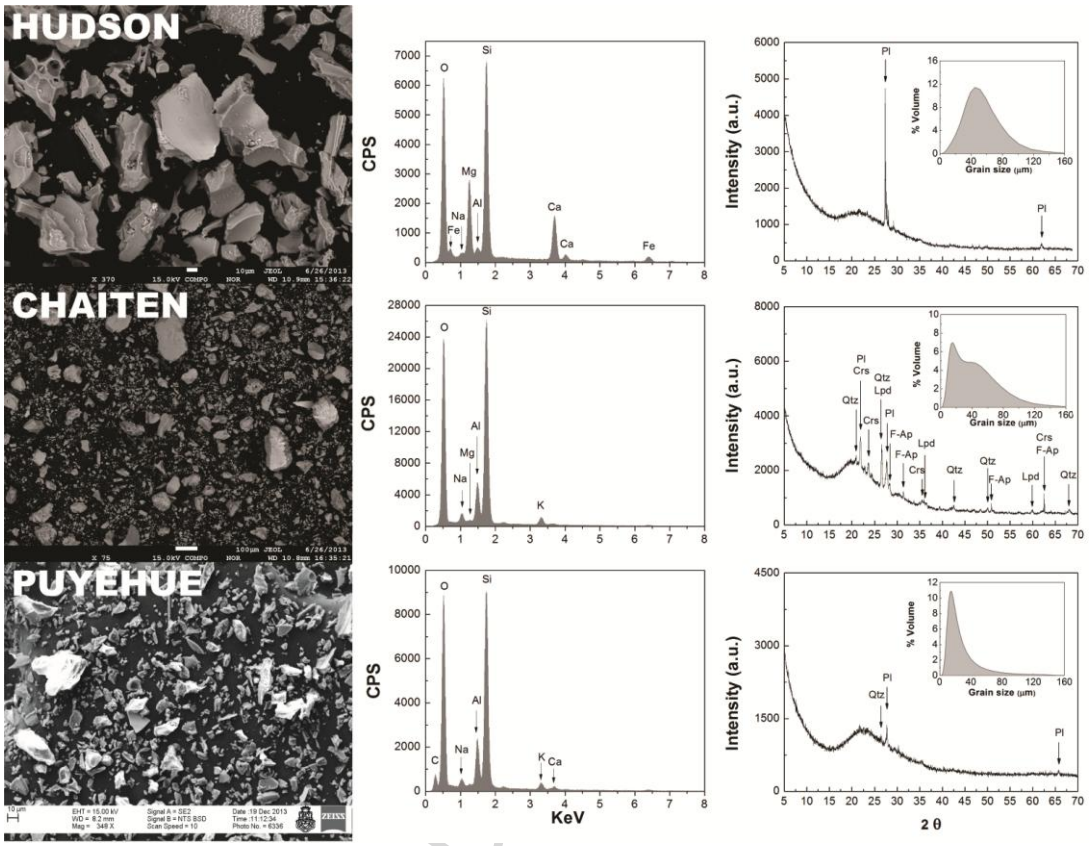

Figure 2

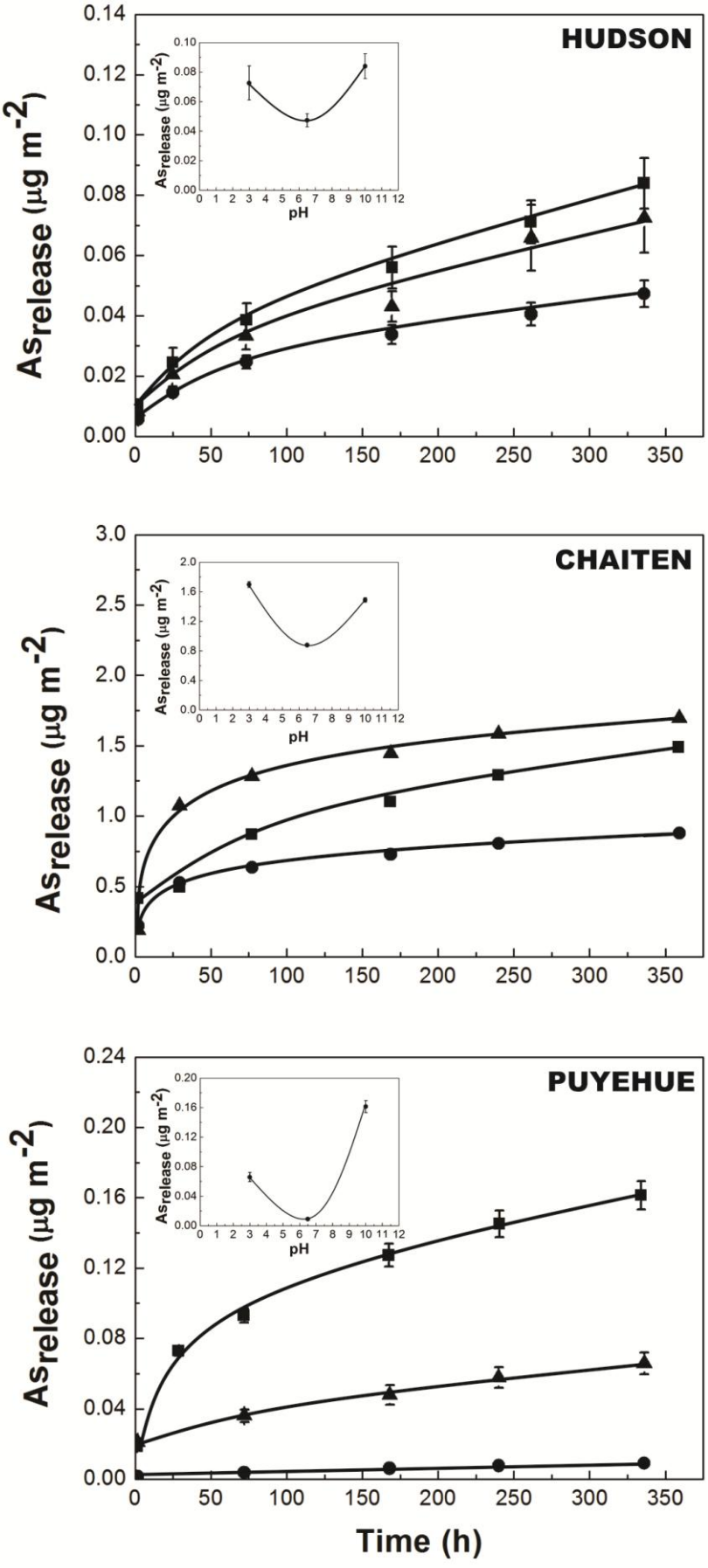

Figure 3

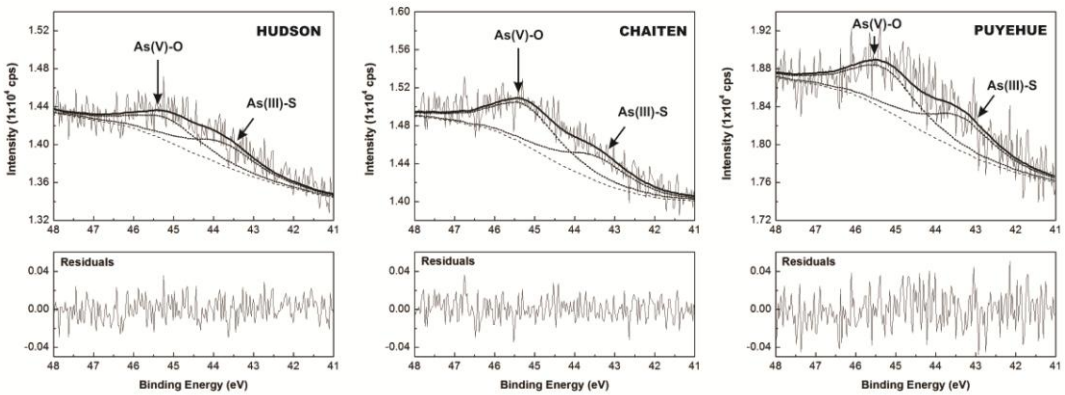

Figure 4

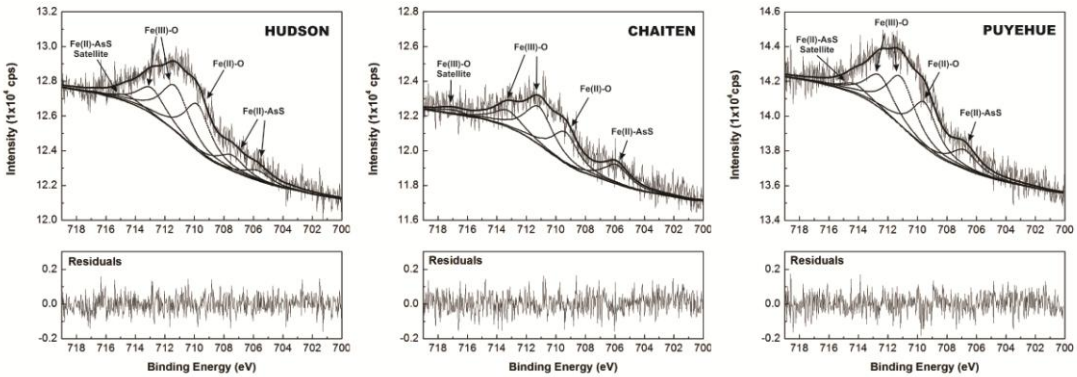

Figure 5

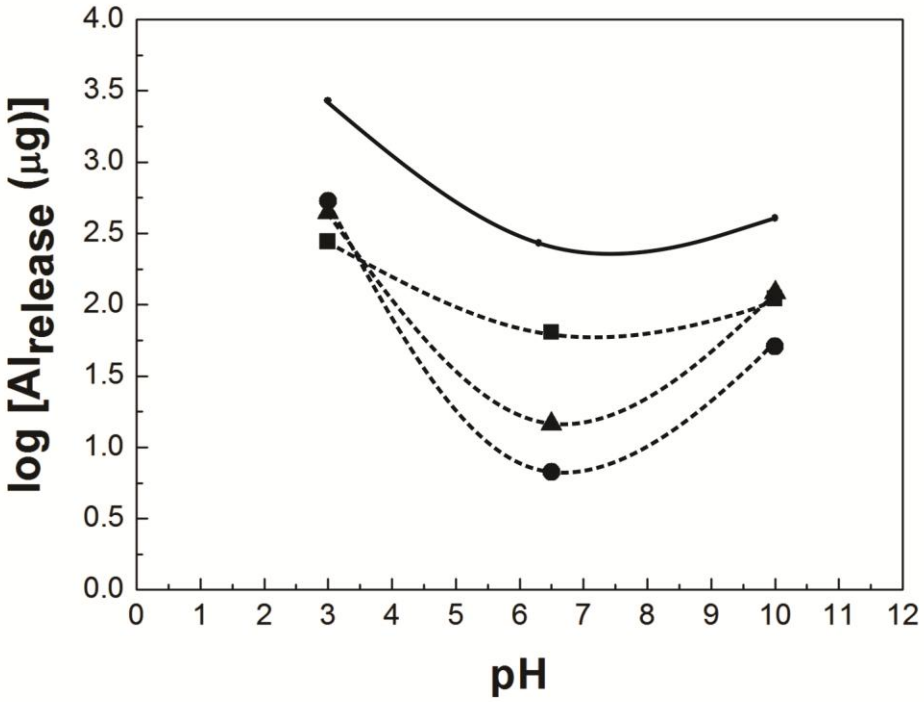

Figure 6

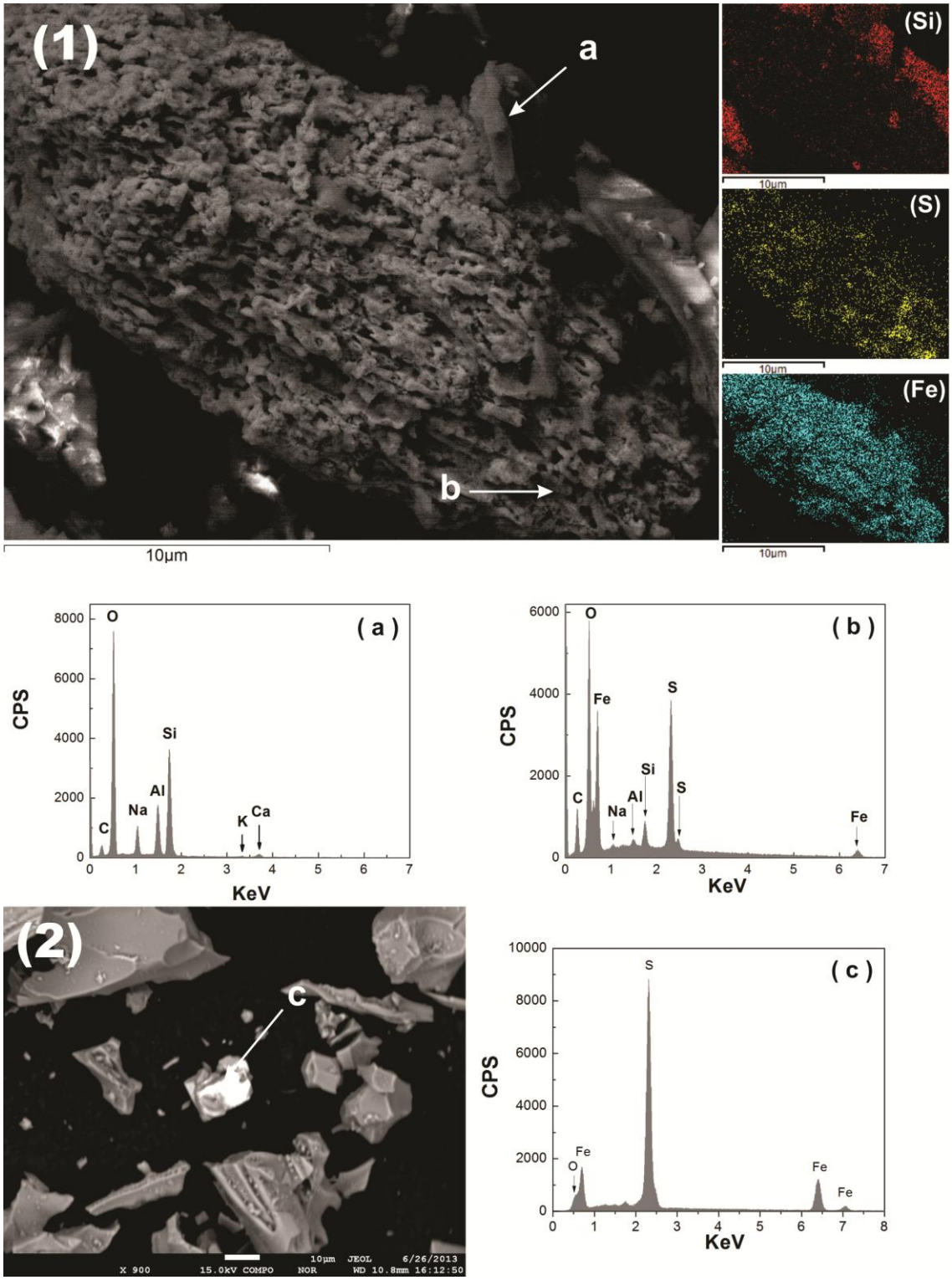

Table 1

Samples	HUDSON	CHAITEN	PUYEHUE
Chemical composition (%)			
SiO_2	59.32	72.45	68.62
Al_2O_3	15.59	13.88	13.27
Fe_2O_3	6.33	1.81	4.4
Na_2O	5.69	4.07	5.2
CaO	3.65	1.74	2.05
K_2O	2.36	2.88	2.82
MgO	1.65	0.46	0.65
TiO_2	1.223	0.175	0.599
MnO	0.163	0.067	0.111
P_2O_5	0.48	0.09	0.09
As concentration (ug g^{-1})	10.0	40.0	15.0
SSA (m^2g^{-1})	2.31	2.62	3.44
% glass	78.0	74.0	88.8

Table 2

Samples	HUDSON			CHAITEN			PUYEHUE		
Chemical composition	**Bulk**	**Surface**	**S/B**	**Bulk**	**Surface**	**S/B**	**Bulk**	**Surface**	**S/B**
Si	52.17	58.78	**1.1**	66.64	64.77	1.0	61.85	68.89	**1.1**
Al	15.53	19.55	**1.3**	14.46	17.90	**1.2**	13.54	14.53	1.0
Na	7.94	8.04	1.0	5.94	5.81	1.0	7.44	4.40	0.6
K	3.69	ND	-	4.70	ND	-	4.51	ND	-
Mg	1.87	3.70	**2.0**	0.55	3.88	**7.0**	0.76	1.31	**1.7**
Fe	8.33	4.10	0.5	2.49	2.46	1.0	5.93	3.84	0.6
Ca	4.91	3.54	0.7	2.45	3.55	**1.5**	2.83	4.20	**1.5**
As	0.0019	0.72	**379**	0.0079	0.80	**101**	0.0029	0.99	**341**
Cl	ND	0.69	-	ND	0.55	-	ND	1.22	-
F	0.009	0.47	**52**	0.0040	0.27	**67**	0.022	0.62	**28**
P	0.39	0.41	1.0	0.077	BDL	-	0.076	BDL	-
S	ND	ND	-	ND	ND	-	ND	ND	-
Ti	1.38	ND	-	0.21	ND	-	0.69	ND	-
Mn	0.24	ND	-	0.10	ND	-	0.17	ND	-
Total	96.46	100.00		97.63	100.00		97.82	100.00	

Table 3

As $3d_{5/2}$ Binding energy (eV)			Designation
Hudson	**Chaitén**	**Puyehue**	
43.7			As(III) in oxidized FeAsS surface
	43.4	43.4	As(III)-S
45.1	45.2	45.3	As(V)-O
Fe $2p_{3/2}$ Binding energy (eV)			**Designation**
Hudson	**Chaitén**	**Puyehue**	
705.7 707.7	705.9	706.8	Fe(II)-AsS
º714.6		714.2	Fe(II)-AsS Satellite
709.8	709.4	709.9	Fe(II)-O
711.3 712.9	711.2	711.1 712.6	Fe(III)-O
	713.3		Fe(III)-O in oxidized FeAsS, surface
	717.0		Fe(III)-O Satellite

Table 4

Species	Binding energy (eV)	Designation	Reference
As^{3+}	43.4	As(III)-S in sulphide minerals	Fullston et al., 1999 Kim et al., 2014
	44.5	As(III)-O in oxidized FeAsS surface	Nesbitt et al., 1995
As^{5+}	45.3	As(V)-O in oxidized FeAsS surface	Nesbitt et al., 1995
	45.4	As(V)-O in As_2O_5	Costa et al., 2002
Fe^{2+}	706-708	Fe(II)-AsS in oxidized FeAsS, surface	Nesbitt et al., 1995
	714.6	Fe(II)-AsS Satellite in oxidized FeAsS surface	Nesbitt et al., 1995
	709.5-709.9	Fe(II)-O in FeO	McIntyre and Zetaruk, 1977 Descostes et al., 2000 Costa et al., 2002
Fe^{3+}	710.4-713.5	Fe(III)-AsS in oxidized FeAsS, surface	Nesbitt et al., 1995
	711-713	Fe(III)-O in Fe_2O_3	Descostes et al., 2000 Biesinger et al., 2011
	717-719	Fe(III)-O Satellite in Fe(III) oxides	Mills and Sullivan, 1983

Table 5

Samples	Volume of tepha (km^3)	Density ($g\ cm^{-3}$)	Estimated mass of delivered As (mt)	Amount of As released (mt)		% As released	
				1.5 h	14 days	1.5 h	14 days
HUDSON	~ 4.30	3.000	1.29×10^5	172.6	1410.0	0.13	1.09
CHAITEN	~ 0.15	0.997	5.98×10^3	86.2	344.2	1.44	5.75
PUYEHUE	~ 0.12	2.200	3.96×10^3	1.5	8.2	0.04	0.21

Highlights

- Volcanic ashes from South Andean volcanoes release As when exposed to water
- As-bearing phases are concentrated onto the ash surface
- As(III)-S species have been assigned to arsenian pyrite
- As(V)-O compounds correspond to arsenate adsorbed or precipitated
- As included within the glass structure is released under extreme pH conditions